Technical Note

Bearing behavior and failure mechanism of a shallow foundation located on/behind the crest of a poorly cemented artificial sandstone

J.C. Chang, J.J. Liao*, Y.W. Pan

Department of Civil Engineering, National Chiao Tung University, 1001 Ta Hsueh Road, HsinChu, Taiwan

1. Introduction

Shallow footing located on/behind the crest of a slope is encountered frequently. To reduce the cost and to improve the performance of structure supports, structures are usually placed on the slope crest or at a setback distance from the slope crest. However, the bearing capacity of such foundations may be reduced because of the influence of the slope. The understanding of the bearing behavior and failure mechanism of the geo-material under a footing foundation under such conditions is essential.

In general, the bearing-failure mode of a foundation on soil depends on soil compressibility and loading type. These types of failure mechanisms are essentially plastic in nature. On the other hand, the bearing-failure mode of a footing foundation on rock can be attributed to the discontinuities or the intact rock properties in a rock mass [1]. Landanyi [2] studied the punching failure of a non-porous brittle rock; he observed various fracturing stages as the bearing pressure approached the ultimate bearing capacity. These fracturing stages included initiation, growing, and finally coalesce forming, which resulted in the areas of crushed rock. Unlike foundations on soil, the feature of the failure mechanism of rock is essentially brittle.

For many young and poorly cemented rocks, the function of lithification with particle cementation and perfect lock-up cannot be achieved due to short period of lithification age [3]. The poorly cemented rock commonly observed in the northern and western foothills of Taiwan is a typical example of this type of geo-material. It usually displays distinctive engineering characteristics including

poor cementation, low bearing capacity, and high deformability [4]. Many researchers [5–7] have suggested that the poorly cemented rock could be considered as a marginal geo-material (between soils and brittle rocks) that may exhibit both plastic and brittle characteristics. Recently, the present authors [8] conducted load-bearing model tests for shallow footing located on the level ground of a poorly cemented sandstone. The model tests used artificial rocks, which reasonably simulate the natural poorly cemented sandstone. The results reveal the load-bearing behavior and failure mechanism of poorly cemented sandstone, with both plasticity and brittle characteristics, is distinct from the cases on hard rock or soil. Consequently, the bearing capacity formulas commonly used for soil or hard rock may not be suitable for the poorly cemented soft sandstones.

For soil slopes, a number of researchers conducted laboratory load-bearing model tests [9–14] or large-scale field load-bearing tests [15]. The experimental results enabled the development and verification of a variety of the bearing capacity theories of shallow foundation on a sloping ground in soil [16–25]. Studies on the subject of shallow foundation on sloping ground in rock, however, are relatively limited. Serrano and Olalla [26] formulated the ultimate bearing capacity for footing on sloping ground in rock. To the authors' knowledge, however, very few studies have reported on the subject of model test of shallow foundation on sloping ground in soft rock.

The present work aimed to investigate the loading behavior and failure mechanism of shallow foundation on/behind the crest of a poorly cemented sandstone slope. Due to its poor cementation, soft rock tends to degrade and lose its strength during sampling. As a consequence, it is difficult to obtain undisturbed samples for those soft rocks with poor cementation. Furthermore, in-situ

*Corresponding author. Tel.: +886 3 5731939; fax: +886 3 5716257.
E-mail address: jjliao@mail.nctu.edu.tw (J.J. Liao).

Table 1
Physical indices of the artificial and natural rocks

	Specific gravity Gs	Wet density ρ_m (g/cm^3)	Air-dried water content ω (%)	Dry density ρ_d (g/cm^3)	Porosity n (%)
Artificial rock	2.62	1.88	2.68	1.85	21.21
Natural rock	2.65	1.96	1.97	1.92	27.50

Table 2
Mechanical properties of the artificial and natural rocks

Mechanical property	Artificial rock	Natural rock	S_f
Uniaxial compressive strength σ_c (MPa)	2.12	3.21	1.51
Strain at failure ε_f (%)	1.17	1.07	0.91
Secant modulus at 50% of σ_c E (MPa)	216.5	286.4	1.32
Modulus ratio E/σ_c	92.13	95.15	1.03
Tensile strength (Brazilian test) σ_t (MPa)	0.24	0.30	1.25
Strength ratio σ_c/σ_t	11.3	10.7	0.95
Cohesion ([a]triaxial compression) c' (MPa)	0.48	0.71	1.48
Friction angle ([a]triaxial compression) ϕ' (deg)	47	50.5	1.07

[a]The confining pressures (σ_3) are 0.1, 0.2, 0.4 MPa.

stratification and random fissures may also result in the heterogeneity and properties' variation of a natural soft rock. To ensure consistent mechanical behavior and reproducible properties of the tested materials, the present study made use of artificial soft rock for the model tests. The artificial rock simulated the Pleistocene poorly cemented sandstone in the northern foothill of Western Taiwan. Details of the experimental set-up, preparation for model specimen, and procedures of load-bearing tests can be referred to [8]. As shown in Tables 1 and 2, the comparison of various properties reveals that the artificial material can reasonably simulate the targeted natural poorly cemented sandstone. A series of load-bearing model tests of strip footing on the slope crest with various slope angles of 10°, 20°, and 30° were conducted. Besides, model tests for different locations of strip footing (at setback distances of 1 and 2.5 footing widths from the slope crest, respectively) were carried out for 20° slopes. In each model test, the bearing behavior and failure mechanism were carefully observed and characterized.

2. Experimental results and discussions

2.1. Consideration of model size

The present authors conducted numerical simulations in order to evaluate the proper size of the tested model prior to the design of the model test [8]. In this study, the size of the strip footing (B) is 50 mm in width; the ratio of specimen size to the strip footing width was 12. The photographs of post-failure specimens in Fig. 1 show the extent of failure zones. The width of the failure zone was about six or seven times of the footing width in the lateral direction; its depth was less than twice of the footing width.

It appears that the effect of boundary confinement on the tested specimens can be ignored.

2.2. Effect of slope angle on load-bearing behavior

For purpose of comparison, the results of load-bearing model tests for strip footing on level ground are also included to examine the influence of slope angle and setback distance on load-bearing behavior and failure mechanism. Details of the experimental results can be referred to [8]. The average ultimate bearing capacity of strip footing on level ground was 10.46 MPa and was taken as a reference. Fig. 2 shows the relation of the ultimate bearing capacity against slope angle. The mean values of ultimate bearing capacity for the strip footing on the slope crest of 10°, 20°, and 30° slopes, respectively, were 9.53, 7.83, and 6.66 Mpa, corresponding to 91%, 75%, and 64%, respectively, of the ultimate bearing capacity for the strip footing on level ground. Evidently, the ultimate bearing capacity decreases with the increase in the slope angle.

Figs. 3–5 show the load–settlement curves and progressive development of fractures during loading. The results indicate that the load–settlement curve can be divided into four stages, i.e., the stress-adjusting stage (between the origin and point A), the linear stage (between points A and B), the non-linear stage (between points B and C), and the ultimate stage (at point C). The photographs taken during the test were carefully examined in order to recognize the progressive failure process and crack development. Fig. 6 illustrates the failure process and crack development in various stages on the load–settlement curve. The crack developments for each stage are described and discussed as follows.
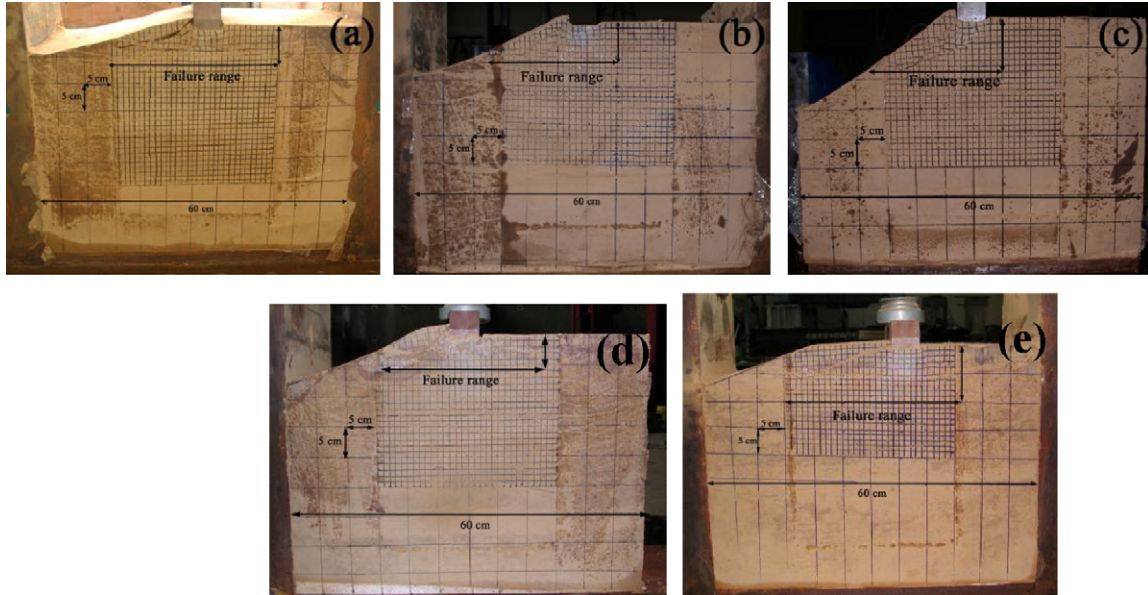
Fig. 1. Typical specimens after load-bearing model test for (a) 10° and slope crest case, (b) 20° and slope crest case, (c) 30° and slope crest case, (d) 20° and setback distance 1B case, and (e) 20° and setback distance 2.5B case.
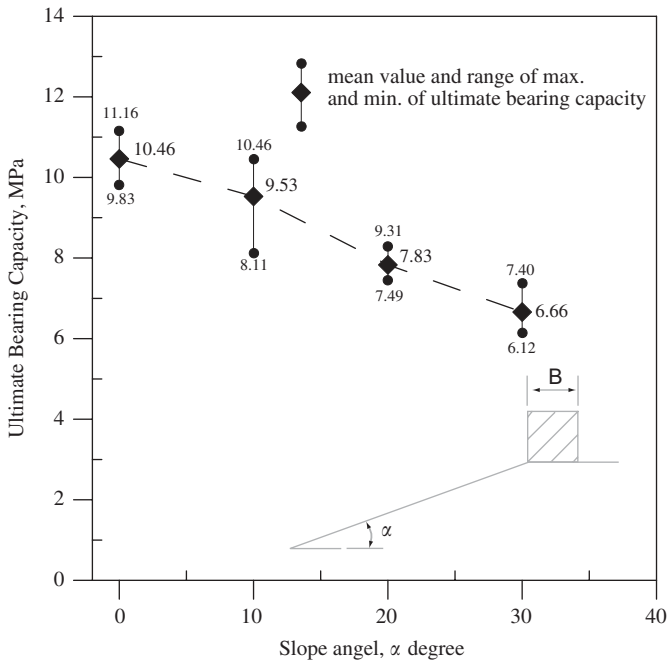

Fig. 2. The variation of ultimate bearing capacity with the slope angle.

At the stress-adjusting stage, the rigid footing and its underneath material gradually developed full contact, and resulted in a concave segment in the initial load–settlement curve. No fissure or crack was observed from the observation window during this stage.

Into the linear stage, as shown in Fig. 6, the stress concentration gradually increased on the fringes of footing and produced cracks. Starting from the left edge of footing, the first crack would gradually propagate and grow with increasing load. After that, the second crack appearing from the right edge of footing was observed with increasing settlement. As the settlement increased, the growing of the initial cracks starting from the right edge of the footing for the cases of 10° and 20° slope was more obvious than that for the case of 30° slope. For the case of 30° slope, it is obvious that the initial cracks starting from the left edge of footing grew visibly more than those starting from the right edge of the footing. These cracks extended outward with increasing load; yet the load–settlement curve remained linear. In this stage, referring to the case of footing on level ground, the initial crack would occur at both edges of the footing simultaneously.

Entering the non-linear stage, the slope of the curve decreased rapidly with increasing settlement of strip footing. At this stage, the initial cracks began to grow rapidly and some new micro-cracks could also be observed. Referring to the grids marked on the specimen surface beneath the base of the footing, it was clear that the foundation material beneath the footing deformed plastically downward and also gradually moved laterally toward the sloping side. As shown in Fig. 6, the initial crack initialing from the left edge of the footing continuously grew and approached the sloping ground. The growing of initial cracks initialing from the right edge of the footing with increasing settlement for the 10° slope was more obvious than that of 20° and 30° slopes. For the 30° slope, the crack initialing from the left edge of the footing propagated toward the slope and finally resulted in a sliding block while approaching the ultimate failure stage. However, the production of this sliding block did not cause the foundation collapse immediately. The cracks appearing under the right edge of the footing began to grow when entering the non-linear stage. As a remark, cracks that
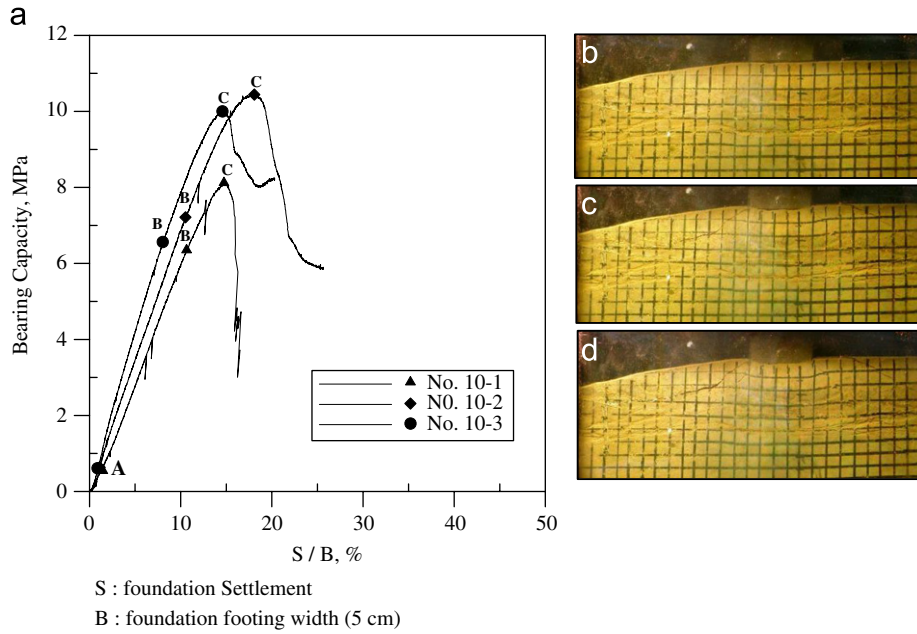
Fig. 3. (a) Load–settlement curve, and progressive development of fractures during loading of 10° case at (b) linear stage starting point as marked A, (c) yielding stage starting point as marked B, and (d) ultimate failure at point as marked C.
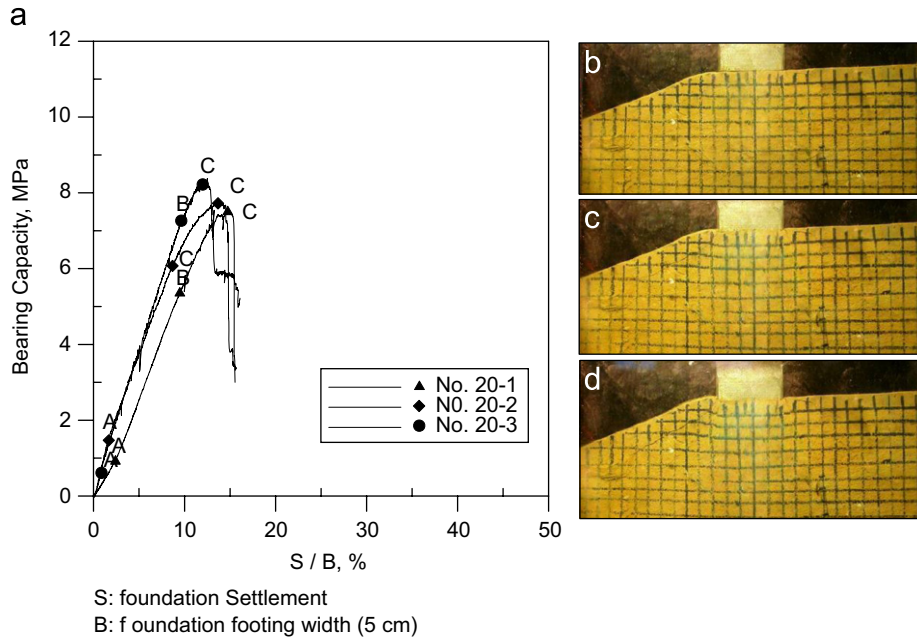

Fig. 4. (a) Load–settlement curve, and progressive development of fractures during loading of 20° case at (b) linear stage starting point as marked A, (c) yielding stage starting point as marked B, and (d) ultimate failure at point as marked C.

occurred in the case of level ground appeared fully symmetrical with respect to the footing center in this stage.

At the ultimate stage, the bearing pressure reached the peak load, and began to decrease abruptly with increasing settlement. For the cases of 10° and 20° slope, the crack initialing from the left edge of the footing (denoted as "crack A") propagated into the slope surface and resulted in the total loss of passive support. As a result, the foundation collapsed and the foundation material de-

formed laterally toward the sloping side. For the case of 30° slope, crack A grew into an upper sliding block and began to overturn and slide. Also, another crack initialing from the left edge of the footing (denoted as "crack B") grew toward the slope surface and resulted in an unstable mechanism in the sloping side, thus causing the foundation collapse. Once a fully connected failure surface was created, the foundation material began to push toward the sloping side, slide outward, and produce more cracks.
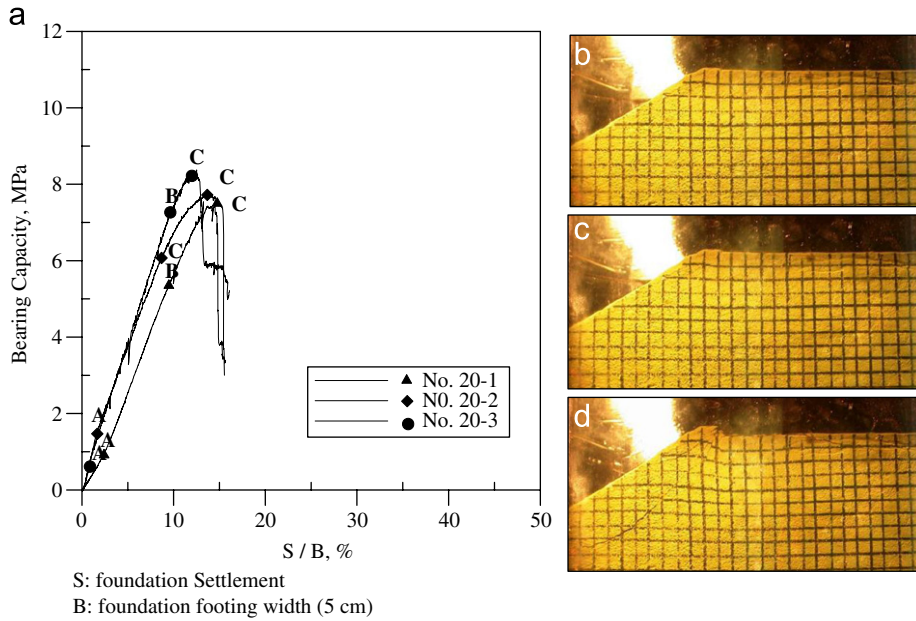
Fig. 5. (a) Load–settlement curve, and progressive development of fractures during loading of 30° case at (b) linear stage starting point as marked A, (c) yielding stage starting point as marked B, and (d) ultimate failure at point as marked C.
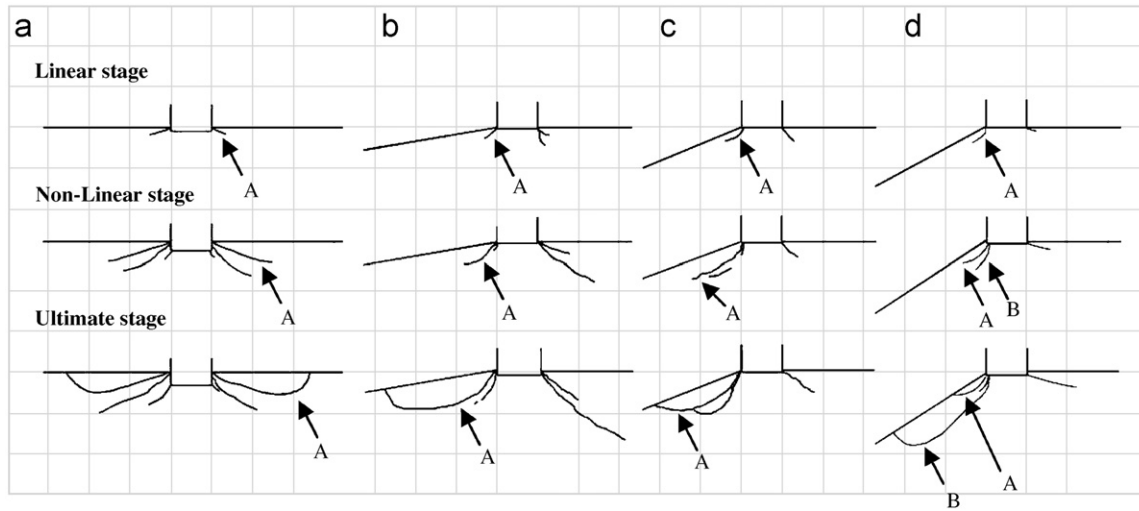

Fig. 6. Illustration of the progressive failure process in various stages for (a) 0° case, (b) 10° case, (c) 20° case, and (d) 30° case.

The stage of the foundation collapse would take place in a very short time. For comparison, the fracture surfaces under the two sides of the footing on the level ground were symmetrical and propagated onto the ground surface, which then resulted in the foundation collapse.

From the comparison of the results of model tests, the ultimate bearing capacity consistently decreases as the slope angle increases. The period of failure process also decreases with increasing slope angle. Unlike the level ground case, the failure mode was not symmetrical and only developed in the sloping side. Observing Fig. 6, it appears that the failure processes for the 10° and 20° slopes are very similar. During the linear stage, crack A starting at the left edge of the footing propagated with increasing load. As crack A propagated onto the slope surface at the

ultimate bearing stage, the foundation collapsed. On the other hand, for the 30° slope, the foundation collapse was due to the situation that crack B extended onto the slope surface instead of crack A. When crack B extended onto the sloping ground, the failure surface developed more rapidly than the cases of 10° and 20° slopes.

For a further examination, a series of slope stability analyses using FLAC_SLOPE that treated soft rock as a Mohr-Coulomb elasto–plastic material with the mean strength parameters (as showing in Table 2) were carried out. The failure footing load that would result in sliding failure corresponding to the safety factor of 1.0 was obtained through these analyses. From the numerical results, provided sliding failure occurred, the failure load for the strip footing on the slope crest of 10°, 20°, and 30°

slopes, respectively, should be 70, 46.5, and 39 MPa (corresponding to 735%, 594%, and 586%, respectively, of the ultimate bearing capacity from the load-bearing experiments). It implied the failure mechanism of the load-bearing model tests was due to foundation collapse, not slope failure. As shown in Fig. 7, the failure surfaces of 10° and 20° slopes were very similar and relatively deep. The

failure surface of 30° slope, on the other hand, was different from those of 10° and 20° slopes and was relatively shallow. From the results of model tests and numerical studies, it may be inferred that failure process is affected by the slope angle, especially when slope angle is greater than 30°.

2.3. Effect of setback distance on load-bearing behavior

In addition to the series of model tests for footing located at slope crest, another series of load-bearing model tests for footing located on various setback distances from 20° slope crest were conducted to study the effect of setback distance. Fig. 8 shows the relationship of ultimate bearing capacity against setback distance. It appears that the ultimate bearing capacity increases with increasing setback distance. The mean values of ultimate bearing capacity for the strip footing located on the setback distance B and $1.5B$, respectively, were 8.38 and 10.09 Mpa, corresponding to 80% and 96%, respectively, of the ultimate bearing capacity for the strip footing on level ground. Hence it is inferred that the ultimate bearing capacity for a footing at a setback distance large than $2.5B$ may be close enough to that in the level ground case.

As shown in Figs. 9 and 10, the load–settlement curves are very similar to the case of footing on the 20° slope crest, and can also be divided into the same four stages. Fig. 11 shows the failure process and crack development during various stages on the load–settlement curve. The failure behavior of the stress-adjusting stage was similar to the corresponding one described in Section 2.3. During the linear stage, the cracks starting from the fringes of footing
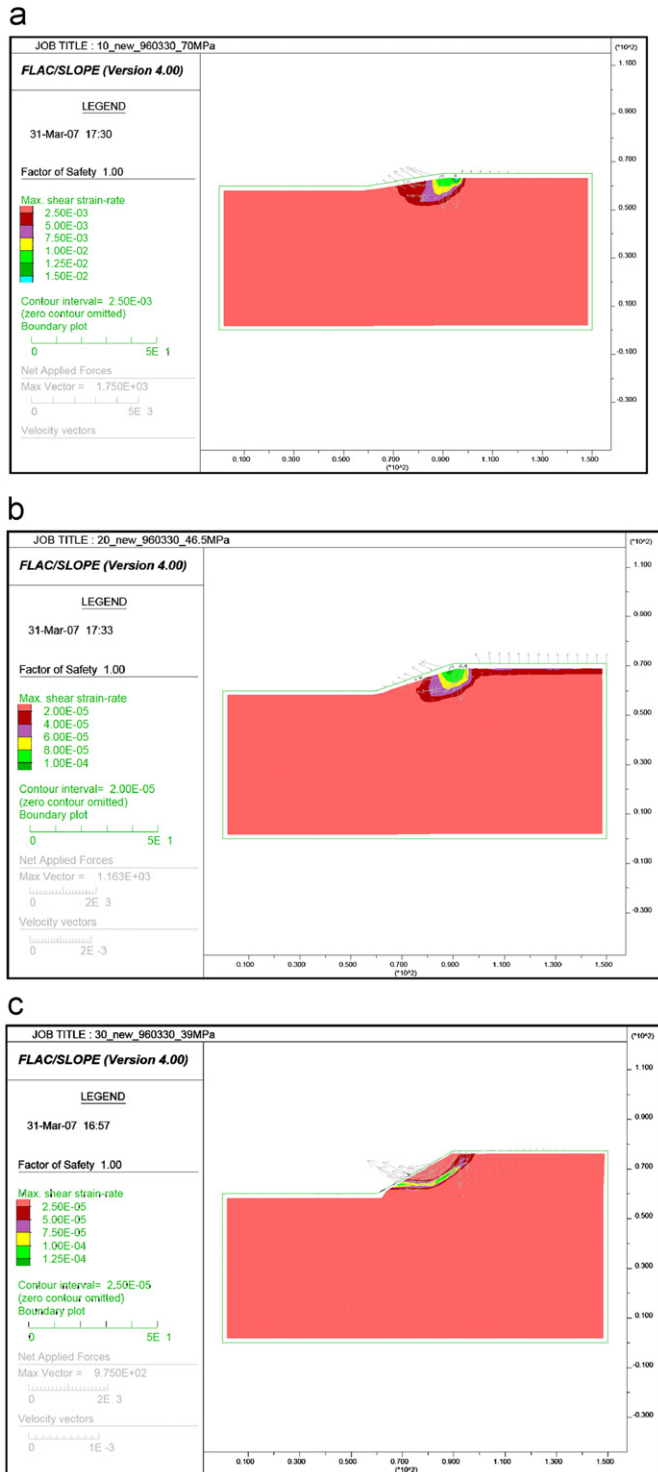

Fig. 7. Failure surface of sliding failure, when safe factor was 1, for (a) 10° case, 70 MPa, (b) 20° case, 46.5 MPa, and (c) 30° case, 39 MPa.
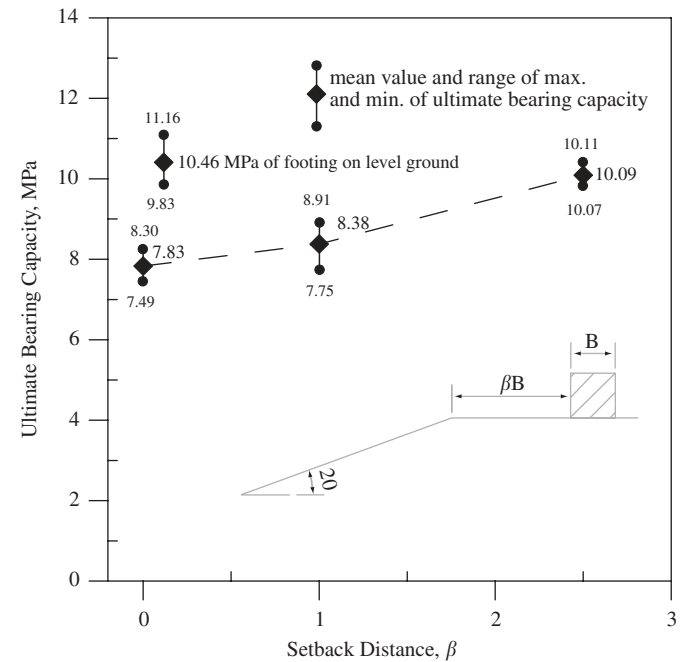

Fig. 8. The variation of ultimate bearing capacity with the setback distance.
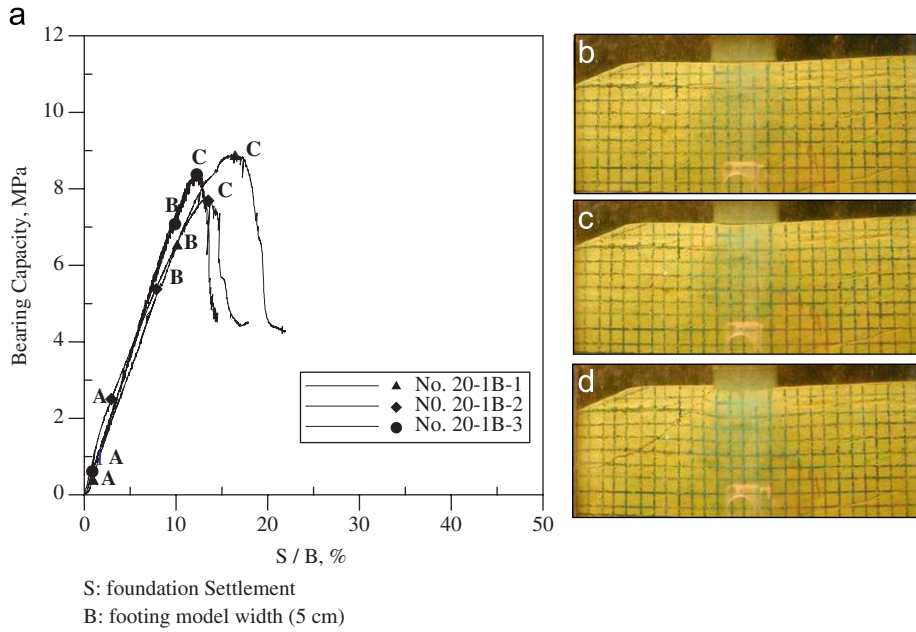
Fig. 9. (a) Load–settlement curve, and progressive development of fractures during loading of setback distance 1*B* case at (b) linear stage starting point as marked A, (c) yielding stage starting point as marked B, and (d) ultimate failure at point as marked C.

Fig. 10. (a) Load–settlement curve, and progressive development of fractures during loading of setback distance 2.5*B* case at (b) linear stage starting point as marked A, (c) yielding stage starting point as marked B, and (d) ultimate failure at point as marked C.
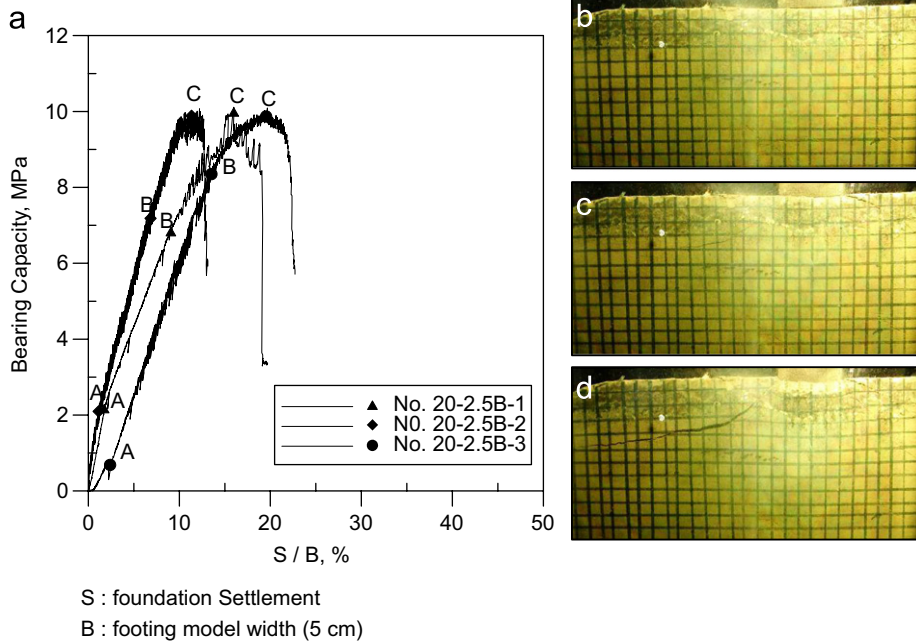
due to stress concentration grew with increasing load and the load–settlement curve remained linear. The growth of a crack starting from the right edge of the footing was more obvious when the setback distance was larger. During the non-linear stage, the slope of load–settlement curves decreased rapidly and the foundation material beneath the footing deformed plastically downward and laterally. At this stage, the initial cracks began to grow rapidly and new cracks could also be observed near the footing base. At

the ultimate stage, the bearing pressure reached the peak load and began to decrease abruptly with increasing settlement. The period of failure process increased with increasing setback distance. As shown in Fig. 11, crack A initialing from the left edge of the footing propagated onto the slope surface and resulted in the final collapse.

The form of failure surfaces was affected by the setback distance from the slope crest. It was observed that the length of crack A in the ultimate stage tends to increase
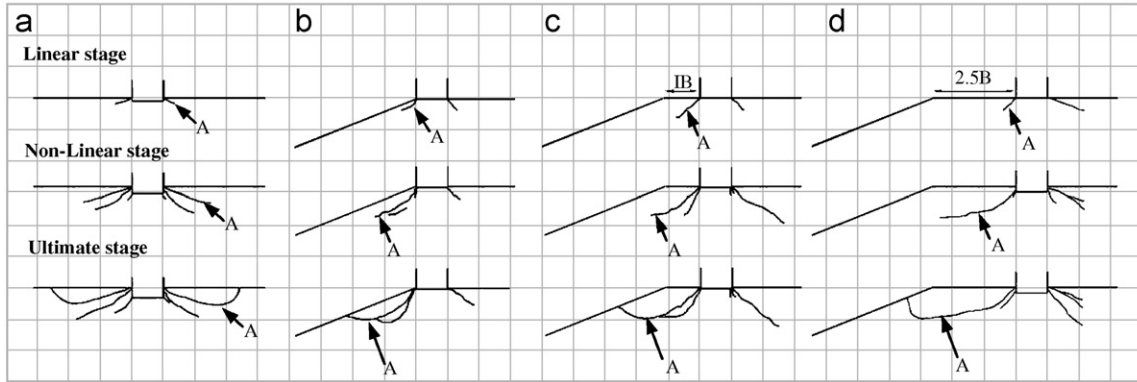
Fig. 11. Illustration of the progressive failure process in various stages for (a) 0° case, (b) 20° and slope crest case, (c) 20° and setback distance 1*B* case, and (d) 20° and setback distance 2.5*B* case.
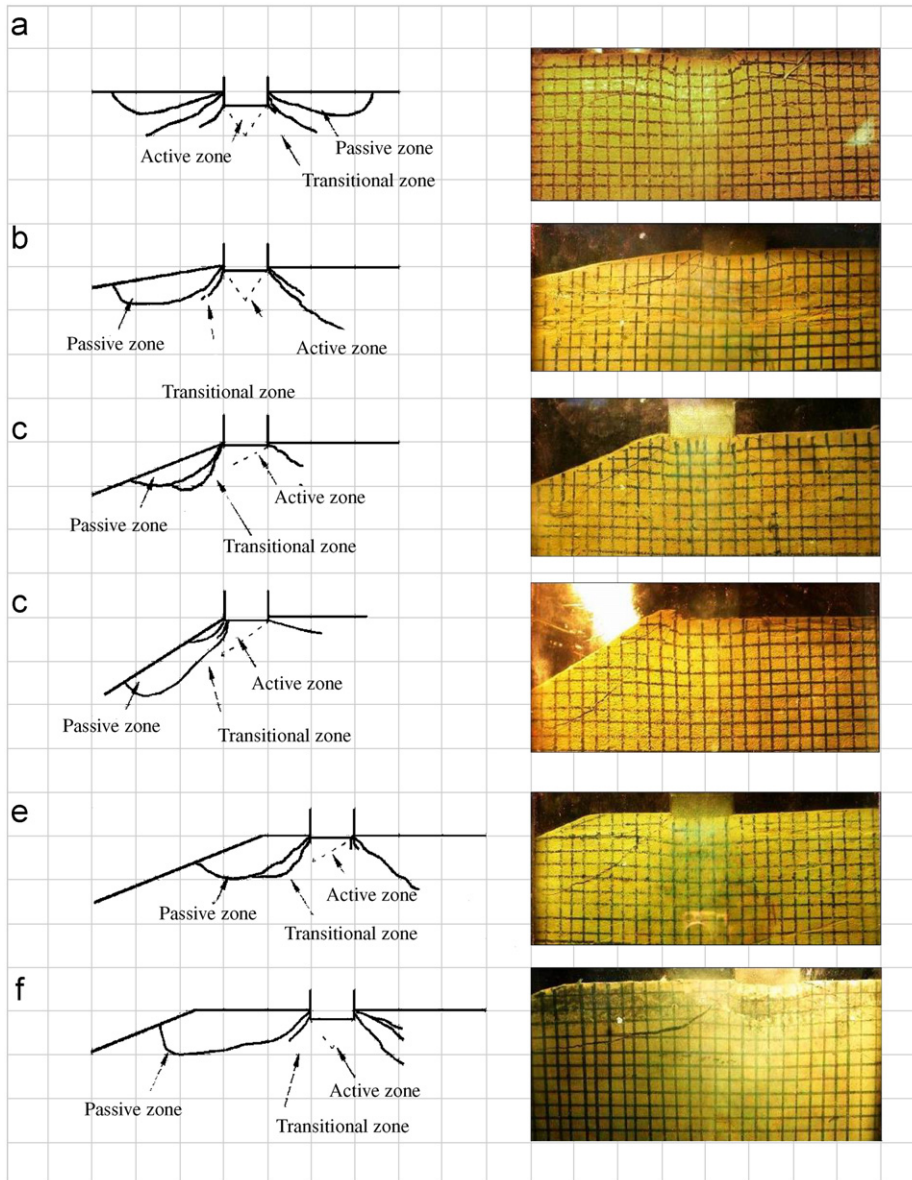

Fig. 12. Failure mechanisms and photographs of ultimate failure for (a) 0°case, (b) 10° and slope crest case, (c) 20° and slope crest case, (d) 30° and slope crest case, (e) 20° and setback distance 1*B* case, and (f) 20° and setback distance 2.5*B* case.

with increasing setback distance; as a consequence, the failure zone was larger and would provide a higher bearing capacity. It is interesting to note that even the failure model for a setback distance of 2.5B was more or less influenced by the slope, although the ultimate bearing capacity had been quite close to that on a level ground. Crack A in the ultimate stage was affected by the slope because the crack still grew on to the slope surface; the fracture surface under two sides of footing was not yet symmetrical.

3. Failure mechanism

Figs. 12 (a–f) illustrate the failure modes and photographs taken right at the ultimate stage, as marked C on the load–settlement curves. The displayed failure mode was drawn on the basis of real-time observation and examination through the photographs taken during tests. At the ultimate state for all tests, the failure zones were composed of three distinct zones, including the active zone under the footing base, the passive zone in the sloping side, and a transition zone containing one or two radial cracks in between active and passive zones. Unlike the level ground case, the failure zones were not symmetrical and only developed in the sloping side.

The active zone, in the shape of an inverted triangle, exists under the footing base. It is noted that, as the slope angle increases and setback distance decreased, the shape of the inverted triangle deformed more toward the sloping side. In the active zone, the foundation material deformed downward and laterally toward to the sloping side. Hence, the vertical stress is the major principle stress σ_1 and the horizontal stress is the minor principle stress σ_3.

The passive zone was formed by crack A or crack B (for footing on a 30° slope crest) starting at the left edge of the footing and finally extended onto the slope surface. The extent of passive zone reduces with increasing slope angle decreasing the setback distance. In the passive zone was pushed laterally and outward. The passive zone is n, the vertical stress is σ_3, and the horizontal stress is σ_1. For a footing located on 30° slope crest, the sliding block formed by crack A is smaller than the passive zone and does not result in the foundation collapse; this small sliding block can be ignored.

A transition zone, which may contain one or two radial cracks that divide this zone into two or three sub-zones, is located between the active and the passive zones. As shown in Fig. 13, the transition zone is composed of stepped-path sliding planes; the sliding plane has a wavy and rough surface. Based on a close-up examination and the fractography concept, the cracks are likely shear cracks rather than tensile cracks. Slickenside was formed due to shearing process. The shear cracks provided stress discontinuities between the active zone and the passive zone; it enables the major principle plane to rotate progressively from the active zone (σ_1 = the vertical stress) to the passive zone (σ_3 = the vertical stress). When the shear fracture composed of the passive zone finally reached the slope
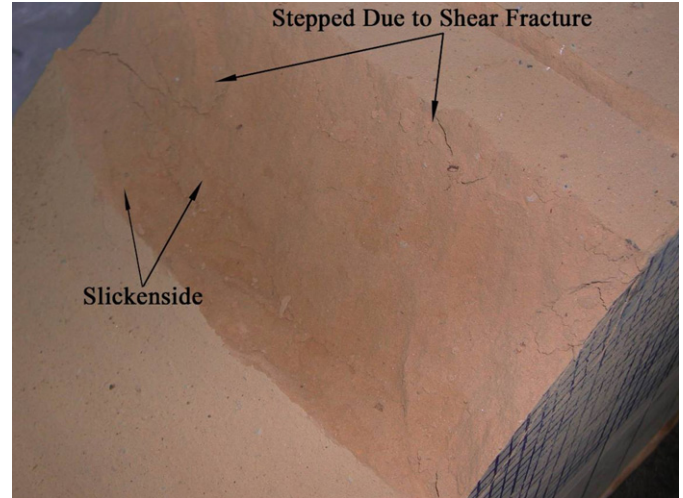

Fig. 13. Fracture planes in the transition zone.

surface, the footing foundation would lose its bearing capacity eventually.

4. Comparison of experimental results and others' investigation

For soil slopes, the experiments in Refs. [9–15] were limited to cohesionless soil or granular sand. These results showed that the failure model could be categorized as perfect plastic failure with a circular slip surface. In common, the failure region was divided into active zone, passive zone, and radial shear zone; however, the radial shear zone was in global shear failure and bounded by a logarithmic spiral line. From the failure mechanism observed in the model tests, it appears that neither conventionally adopted failure mechanisms for soils nor those of rigid rock can fully represent the bearing-failure mechanism on poorly cemented sandstone. The failure mechanism develops both plastic deformation in active zone and the growth of cracks as the slip surfaces in the transitional zone. The pattern and extent of failure zones were affected by slope angle and setback distance, hence largely influencing the corresponding ultimate bearing capacity. The failure mechanism contains several triangular wedges as rigid blocks separated by interfaces and discontinuities; it can be categorized as a type of multi-block translation mechanism.

Attempt was made to compare the experimental results with the calculated results based on some existing theories. As shown in Table 3, the bearing capacity was calculated with the average strength parameter of artificial rock. The solutions of Hansen [25] and Chen [20] over-estimate the bearing capacity to a great extent. The general assumption of global shear failure and failure mechanism in these theories (e.g., [16,20,21,23,24]) may be responsible for this significant over-estimation. Graham [22] used stress characteristics to derive the bearing capacity solution for footing loaded on cohesionless soil slope. These theories

Table 3
Comparison of ultimate bearing capacities based on various theories

Slope condition	Brnich Hansen (1970)	Chen (1975)	Graham (1988)	Serraon and Olalla (1996)
Method of analysis	Limit equilibrium method	Limit analysis	Characteristics method	Characteristics method
Required strength parameters	γ, c, ϕ	γ, c, ϕ	γ, ϕ	σ_c, RMR, m, s
Calculated q_u for 10° and slope crest (MPa)	57.1 (599%)	57.2 (600%)	0.2 (2%)	35.63 (374%)
Calculated q_u for 20° and slope crest (MPa)	34.1 (436%)	39.2 (501%)	0.1 (1%)	–
Calculated q_u for 30° and slope crest (MPa)	15.0 (255%)	26.8 (402%)	0.05 (0.8%)	–
Calculated q_u for 20° and setback distance 1B (MPa)	–	–	0.2 (2%)	–
Calculated q_u for 20° and setback distance 2.5B (MPa)	–	–	0.24 (2%)	–

Difference ratio = (calculated value/average experimental value) × 100%.

[17,22] assumed that the cohesion of soil is negative; they only take the weight of material into account. Experimental results were also compared with the solution of ultimate bearing capacity with the nonlinear Hoek–Brown failure criterion by assuming RMR = 100, $m = 12$ and $s = 1$. The bearing capacity solution of Serrano and Olalla [26] was related to uniaxial compressive strength; however, this mechanism differs from our experimental observation for foundation on soft rock. These comparisons reveal the importance to capture the actual failure mechanism of footing failure. The experimentally observed multi-block failure mechanism provides the basis for developing the upper bound solution of ultimate bearing capacity in a consecutive study.

5. Summary and conclusions

A series of load-bearing model tests were conducted to study the bearing behavior and failure mechanism of a shallow foundation on/behind a poorly cemented sandstone slope. The model rock slope was made of artificial rock that simulates natural poorly cemented sandstone. The similarity of their mechanical characteristics was examined by similitude comparison. The comparisons confirmed that the properties of the artificial material are close to those of natural poorly cemented sandstone.

The load-bearing behavior can be divided into four stages: the stress-adjusting stage, the linear stage, the non-linear stage, and the ultimate stage on load–settlement curve. The failure zone and mechanism were also identified. The failure mechanism was composed of an active zone, a transitional zone, and a passive zone; the failure zones eventually propagate into the sloping side. Slope angle and setback distance affect the area and shape of failure zones, as a consequence, significantly affecting the ultimate bearing capacity. The results of model tests indicate that the ultimate bearing capacity decreases with increasing slope angle and increases with increasing setback distance. When the setback distance is more than 2.5 times of the width of the footing, the ultimate bearing capacity is close to that of level ground.

The bearing behavior and failure mechanism on poorly cemented sandstone are distinct from the cases of hard rock or soil; it possesses both plasticity and brittle characteristics. Based on the observed behavior from the model tests, the failure mechanism may be modeled as a multi-block translation mechanism.

References

[1] Goodman RE. Introduction to rock mechanics. New York: Wiley; 1989. p. 350–2.
[2] Landanyi B. Quasi-static expansion of cylindrical cavity in rock. In: Proc Int Symp Eng Applic Solid Mech. CSCE & University of Toronto; 1976. p. 219–40.
[3] Barton ME. Cohesive sands: the natural transition from sands to sandstones. In: Proc Symp Geotech Eng Hard Soils–Soft Rocks. Rotterdam: Balkema; 1993. p. 367–74.
[4] Huang AB, Liao JJ, Pan YW, Cheng MH, Hsieh SY, Peng JK. Characterization of soft rocks in Taiwan. In: Proceedings of the fourth North American rock mechanics symposium, Seattle, 2000. p. 83–90.
[5] Johnstone IW, Williams AF, Chiu HK. Properties of soft rock relevant to socked pile design. In: Proc Int Conf Struct Foundations on Rock, Sydney. Rotterdam: Balkema; 1980. p. 55–64.
[6] Dobereiner L, Freitas DE. Geotechnical properties of weak sandstones. Geotechnique 1986;36(1):79–94.
[7] Oliveira R. Weak rock material. In: Proc 26th Ann Conf Eng Group Geol Soc. Rotterdam: Balkema; 1993. p. 5–15.
[8] Chang JC, Liao JJ, Pan YW. Failure mechanism and bearing capacity of shallow foundation on poorly cemented sandstone. J Mech 2008;24(3).
[9] De Beer EE. Experimental determination of the shape factors and the bearing capacity factors of sand. Geotechnique 1970;20(4):387–411.
[10] Lebegue Y. Essais de foundations superficielles sur talus. In: Proceedings of the eighth international conference on soil mechanics and foundation engineering, vol. 4.3, Moscow, 1973. p. 313.
[11] Dembicki E, Zadroga B. Model tests on bearing capacity of foundations on slope. In: Proc of the fourth Danube-European conference on soil mechanics and foundation engineering 1974:147–53.

[12] Bauer GE, Shields DH, Scott JD, Gruspier JE. Bearing capacity of footings in granular slopes. In: Proceedings of the 10th international conference on soil mechanics and foundation engineering, vol. 2, Stockholm, 1981. p. 33–6.

[13] Kusakabe O, Kimura T, Yamaguchi H. Bearing capacity of slopes under strip loads on top surfaces. Soils Foundations 1981;21(4): 29–40.

[14] Gemperline MC. Centrifuge modeling of shallow foundations. In: Proceedings of the ASCE Spring Convention, ASCE 1988.

[15] Shields DH, Scott JD, Bauer GE, Deschenes JH, Barsvary AK. Bearing capacity of foundations near slopes. In: Proceedings of the ninth international conference on soil mechanics and foundation engineering, vol. 2, Tokyo, 1977. p. 715–20.

[16] Meyerhof GG. The ultimate bearing capacity of foundation on slopes. In: Proceedings of the fourth international conference on soil mechanics and foundation engineering, vol. 1, London, 1957. p. 384–6.

[17] Mizuno T, Tokumitsu Y, Kawakami H. On the bearing capacity of a slope of cohesionless soils. Soils Foundations 1960;1:30–7.

[18] Sokolovski VV. Statics of soil media. London: Butterworths; 1960.

[19] Greenstein J, Livneh M. Slip line field of anisotropic soil. J Appl Mech 1974;41(2):453–8.

[20] Chen WF. Limit analysis and soil plasticity. Amsterdam: Elsevier; 1975.

[21] Osamu K, Tsutomu K, Hakuju Y. Bearing capacity of slope under strip loads on the top surface. Soils Foundations 1981;21(4):29–40.

[22] Graham J, Andrews M, Shields DH. Stress characteristics for shallow footings in cohesionless slopes. Can Geotech J 1988;25(2):238–49.

[23] Saran S, Sud VK, Handa SC. Bearing capacity of footings adjacent to slopes. J Geotech Eng ASCE 1989;115(4):553–73.

[24] Bowles JE. Bearing capacity of footing on slopes. In: Foundation analysis and design. 4th ed. New York: McGraw-Hill; 1988. p. 215–9.

[25] Fang HY. Bearing capacity of shallow foundations. In: Foundation engineering handbook. 2nd ed. New York: Van Nostrand Reinhold; 1991. p. 154.

[26] Serrano A, Olalla C. Allowable bearing capacity in rock foundations based on non-failure linear criterion. Int J Rock Mech Min Sci 1996;33(4):327–45.